# Diagnosing the influence of a receding snow boundary on simulated midlatitude cyclones using piecewise potential vorticity inversion

*By*

**Corresponding Author:** Melissa L. Breeden, NOAA Earth System Research Laboratory, Chemical Sciences Division, Boulder CO

Ryan Clare, Naval Research Laboratory, Monterey, CA

Jonathan E. Martin, Department of Atmospheric and Oceanic Sciences, University of Wisconsin-Madison, Madison, WI

Ankur R. Desai, Department of Atmospheric and Oceanic Sciences, University of Wisconsin-Madison, Madison, WI

**Abstract:** Previous research has found a relationship between the equatorward extent of snow cover and low-level baroclinicity, suggesting a link between the development and trajectory of midlatitude cyclones and the extent of preexisting snow cover. Midlatitude cyclones are more frequent 50-350 km south of the snow boundary, coincident with weak maxima in the environmental Eady growth rate. The snow line is projected to recede poleward with increasing greenhouse gas emissions, possibly affecting the development and track of midlatitude cyclones during Northern Hemisphere winter. Detailed examination of the physical implications of a modified snow boundary on the lifecycle of individual storms has, to date, not been undertaken. The present study investigates the impact of a receding snow boundary on two cyclogenesis events using Weather Research and Forecasting (WRF) model simulations initialized with observed and projected future changes to snow extent as a surface boundary condition. Potential vorticity diagnosis of the modified cyclone simulations isolates how changes in surface temperature, static stability, and relative vorticity arising from the altered boundary affect the developing cyclone. We find that the surface warm anomaly associated with snow removal lowered heights near the center of the two cyclones investigated, strengthening their cyclonic circulation. However, the direct effect of snow removal is mitigated by the stability response and an indirect relative vorticity response to snow removal. Due to these opposing effects, it is suggested that the immediate effect of receding snow cover on midlatitude cyclones is likely minimal and depends on the stage of the cyclone lifecycle.

## 1. Introduction

As the planet warms, the climatological southern edge of snow cover during boreal winter and spring is projected to move poleward (Manabe and Wetherald 1980; Brown 2000; Lemke et al. 2007; Gan et al. 2013). Rydzik and Desai (2014) found that there was a statistical relationship between the location of the snow boundary, low-level baroclinicity, and cyclone tracks, presumably related to enhanced radiative, thermal, and moisture gradients along the snow line. Consequently, it is possible that changes in the snow boundary could impact aspects of developing cyclones over the next century.

The large-scale, low-frequency circulation response to receding snow cover has been investigated previously and is nonnegligible. Ross and Walsh (1986) used the National Center for Atmospheric Research (NCAR) Community Forecast Model to force anomalous snow extent over North America, which, months later, induced remote temperature responses over Scandinavia and western Europe. Klingaman et al. (2008) examined the large-scale response to

anomalous Great Plains snow cover imposed in simulations using the Community Atmosphere Model and found a response in Eurasian temperatures related to a positive North Atlantic Oscillation (NAO) that developed at a lag of several months. Sobolowski et al. (2010) examined the low-frequency, large-scale atmospheric response to a persistent snow cover anomaly using a pair of 40-member atmospheric general circulation model simulations with high and low-snow forcing, and also found a transient eddy response in the North Atlantic storm track due to anomalous snow cover over North America.

A separate question that has also received research attention is -- what is the immediate (i.e., occurring within days following production of a snow cover anomaly), regional atmospheric response to snow cover? Using a one-dimensional snowpack model, Ellis and Leathers (1999) simulated the effect of snow removal on four cold air masses that developed in the Great Plains region of the United States. They found that for all four cases, the air masses warmed on average by 6-10°C during the daytime, and by 1-2°C during nighttime, primarily through sensible heat fluxes from the ground to the air mass. Elguindi et al. (2005) compared the intensity and sensible weather associated with cyclogenesis in the Great Plains of North America for cases with the observed snow boundary and for simulations with snow completely covering the model domain. They found that covering the domain with snow led to weaker mean sea level pressure minima, weaker fronts and thermal advection, and reduced precipitation and cloud cover due to weaker vertical motion. Perhaps directly related to the former pair of attributes, increased static stability of the lower troposphere was also characteristic of the snow-covered domain.

Previous research examining how a change in snow cover affects the development of extratropical cyclones has focused on the presence of more-than-typical snow cover and colder than normal temperatures. Whether the tropospheric response and influence on cyclones in the

*absence* of snow and *warmer* than normal temperatures produce an equal and opposite response remains to be determined. In the present study, we have designed modeling experiments to test if the removal of snow will affect the strength and/or trajectory of developing cyclones over North America. The removal of snow is hypothesized to increase low-level temperature and consequently reduce static stability. To isolate the direct and indirect effects snow removal has on the circulation, we applied piecewise quasi-geostrophic potential vorticity (QGPV) inversion. The inversion technique can isolate the geopotential height response to changes in a) surface temperature, b) static stability, and c) low-level relative vorticity, that arise due to the removal of snow. It is reasonable to anticipate that the warm surface temperature anomaly associated with snow removal, manifests itself as a cyclonic QGPV anomaly (Bretherton 1966), and as a result, enhances the circulation of amplifying cyclones. Additionally, we suppose that the vertical structure of the resultant surface warm anomaly will reduce the static stability of the environment near the cyclone, which can enhance vertical motion, cloud cover and precipitation.

The paper is organized as follows. Section 2 describes both the modeling simulations designed to test the immediate impact snow removal has on cyclogenesis as well as the potential vorticity inversion technique used for analysis. Section 3 presents results from two selected cases, including a synoptic overview and results from QGPV inversion. A discussion of results and concluding remarks are offered in Section 4.

## 2. Methodology

To test the hypothesized influence of snow removal on cyclogenesis, a suite of model simulations was designed that uses the observed snow boundary position (the control simulation) and a range of plausible changes to the snow line as projected by climate models (see Clare et al. (submitted) for more details). The difference in geopotential height between the control and

125 modified simulations was calculated throughout the troposphere for each case. The resultant
126 height anomaly fields were then used for piecewise potential vorticity inversion, to isolate and
127 quantify the direct and indirect effects, such as changes in temperature and static stability, the
128 modified snow boundary had on the circulation.

129 *2.1 Simulation Design*

130 We ran simulations using the Weather Research and Forecasting (WRF) model version
131 4.0.3 with 30 km grid spacing for 20 subjectively selected cyclone cases that occurred during
132 boreal winter (November – March; Skamarock et al., 2019). The domain for this study includes
133 the continental United States as well as much of Canada and Mexico and is centered over the
134 Great Plains region. A grid cell was identified as snow covered if the simulated snow mass was
135 at least 5 kg $m^{-2}$, corresponding to a snow depth of about 5 cm assuming a 10:1 snow to water
136 ratio. Output from 14 models of the fifth phase of the Coupled Model Intercomparison Project
137 (CMIP5), using the representative concentration pathway (RCP) 4.5 and 8.5 scenarios, was used
138 to determine a range of possible modifications to the position of the snow boundary by the year
139 2100 that could arise from future changes in greenhouse gas concentrations. Each of the CMIP5
140 models used to determine the ranges of snow boundary retreat applied in this experiment are
141 present in the study of 22 CMIP5 models by Brutel-Vuilmet et al. (2013). They found that
142 though the models did not adequately capture significant long-term snow mass reductions in
143 spring, when ensemble-averaged, the models studied were able to realistically reproduce
144 observed snow water equivalent in the period from 1979-2005. Eight of those models were
145 ultimately excluded from consideration in this experiment as a result of restricted data
146 availability, resolution issues, or large regional biases. The remaining model simulations were
147 sorted based upon their projected changes to the snow boundary. For each simulation, the

148 monthly mean change in the snow line between the 2080-2099 and 1986-2005 periods was
149 determined. The projected changes were then grouped into 10th, 50th, and 90th percentile
150 categories. For each of our selected cases, we ran simulations with each percentile's poleward
151 snow line retreat (10th, 50th, and 90th) applied to the observed snow boundary, as well as a
152 simulation with complete snow removal.

153 Additionally, simulations for each case and percentile of snow line retreat were initialized
154 at a range of 0 to 4 days prior to cyclogenesis at 24 hour intervals, ultimately yielding 500
155 distinct simulations. Information regarding the overall results of all simulations can be found in
156 Clare et al. (submitted). Here, two cyclogenesis cases were selected for in-depth analysis. We
157 chose to compare simulations of these cases initialized 4 days prior to cyclogenesis, and consider
158 differences between the control and 90th percentile simulations, to analyze the strongest response
159 to snow removal while remaining within the range of plausible future changes. Results
160 summarizing the response in all 500 model simulations can be found in Clare et al. (submitted).
161 Model output was interpolated to pressure surfaces at 50 hPa intervals from 1000 – 100 hPa at 6-
162 hourly temporal resolution, and was regridded onto a 1°x1° latitude-longitude grid.

163 *2.2 Anomaly Calculations*

164 We use a potential vorticity inversion approach (described in Section 2.3) that employs
165 geopotential height on pressure surfaces to calculate and invert QGPV. To keep our view of the
166 cases consistent with the inversion framework, we consider the evolution of the surface cyclone
167 on pressure surfaces as well. Using each case's control simulation, the mean state, $\bar{z}$, was defined
168 as the 7-day average over which each selected cyclone developed, corresponding to 0000 UTC 3
169 March 2005 – 1800 UTC 9 March 2005 and 0000 UTC 22 January 1996 and 1800 UTC 28
170 January 1996. To track the geopotential height minimum associated with each surface cyclone,

we calculated geopotential height anomalies, $z' = z - \bar{z}$. The evolution of the surface cyclone was then considered using the 1000 hPa $z'$ fields in each case. To determine the change in the height and temperature fields arising from the imposed retreat of the snow boundary, the control simulation height fields were subtracted from those of the 90th percentile snow removal simulations: $z'' = z_{90} - z_{CTRL}$. Temperature anomalies due to removal of snow were calculated in the same manner: $T'' = T_{90} - T_{CTRL}$.

*2.3 Quasi-Geostrophic Potential Vorticity Inversion*

We used piecewise QGPV inversion to test the hypothesized impact on the geopotential height field of the near-surface temperature anomaly created by removing snow. The QGPV approach is particularly amenable to the present analysis, as the components of QGPV linearly combine to produce the observed geopotential height field. QGPV is defined as the sum of the planetary vorticity, geostrophic relative vorticity, and a function of static stability:

$$q = f + \frac{1}{fo}\nabla^2\phi + f_o \frac{\partial}{\partial p}\left(\frac{1}{\sigma}\frac{\partial \phi}{\partial p}\right) \qquad (1)$$

Where $\nabla^2 = (\frac{\partial^2}{\partial x^2}, \frac{\partial^2}{\partial y^2})$, the two-dimensional Laplacian, $\phi$ represents deviations from the reference atmosphere geopotential, $f$ is the Coriolis parameter, and σ is the reference atmosphere static stability ($\sigma = -\frac{\alpha}{\theta}\frac{d\theta}{dp}$), where α is specific volume. To investigate the changes in QGPV associated with a receding snow line, we calculated QGPV anomalies using the $z''$ and $T''$ fields for each case, and split the anomalies into contributions from relative vorticity and static stability (Eqns 2, 4). Horizontal variations in geopotential manifest themselves in the geostrophic relative vorticity term (Eqn 2), so that in the Northern Hemisphere cyclones are characterized by relative vorticity maxima and positive QGPV anomalies, while anticyclones are characterized by relative vorticity minima and negative QGPV anomalies.

193 $$q''_{\zeta} = \frac{1}{fo}\nabla^2\phi'' \qquad (2)$$

194 The vertical gradient of geopotential is related to temperature, $T$, through the hydrostatic
195 relationship (Eqn 3). As a result, QGPV is also proportional the vertical change of temperature
196 (and temperature anomalies) and therefore to atmospheric stability, with stability maxima
197 corresponding to positive QGPV anomalies and vice versa (Eqn 4).

198 $$\frac{\partial\phi''}{\partial p} = -\frac{R}{p}T'' = -\frac{R}{p}\left(\frac{p}{p_o}\right)^{\kappa}\theta'' \qquad (3)$$

199 $$q''_{st} = f_o\frac{\partial}{\partial p}\left(\frac{1}{\sigma}\frac{\partial\phi''}{\partial p}\right) \qquad (4)$$

200 As such, regions in which temperature decreases rapidly with height are characterized by
201 reduced stability and QGPV minima. Anywhere temperature increases with height (or decreases
202 less rapidly), is, conversely, associated with enhanced stability and QGPV maxima.

203 Bretherton (1966) showed that surface potential temperature (θ) anomalies could be
204 considered QGPV anomalies, and in particular that surface warm (cold) anomalies act as
205 cyclonic (anticyclonic) QGPV anomalies. We include the model-output $T''/\theta''$ anomalies as a
206 Neumann boundary condition at the lower boundary (1000 hPa) via Eqn 3, and solve for the
207 height field without any interior QGPV values, to determine the nonlocal response to the 1000
208 hPa temperature anomalies produced by snow removal. The resultant geopotential anomaly shall
209 be referred to as $\phi''_{\theta}$, and represents the balanced, troposphere-deep height response to the
210 surface $\theta''$ anomaly.

211 Holopainen and Karola (1991) demonstrated that one can partition QGPV anomalies in
212 various ways, including inversion of the relative vorticity, stability and surface temperature
213 components separately or inversion of anomalies within different vertical layers. For our
214 purposes of isolating the surface temperature impact on the circulation, we calculated the QGPV

anomalies associated with surface temperature anomalies, relative vorticity and stability separately. We then determined the nonlocal impact each of these QGPV anomalies has on the circulation by inverting each anomaly separately, to retrieve its associated geopotential height fields (Eqn 5). Inversion was performed using an iterative successive overrelaxation technique.

$$z'' = z''_\theta + z''_\zeta + z''_{st} = \frac{1}{g}\left(\phi''_\theta + \mathcal{L}^{-1}\left(q''_\zeta\right) + \mathcal{L}^{-1}\left(q''_{st}\right)\right) \qquad (5)$$

In this manner, we were able to test our hypothesis regarding the suspected impact of removing snow on the height field near developing cyclones in the two cases examined. There is substantial cancellation between the surface temperature and stability response (which we explore in Section 3), so for brevity we consider these terms as a net temperature/stability height anomaly, $z''_T = z''_\theta + z''_{st}$, in some of the following analysis.

## 3. Results

Two cases were selected for investigation in this study, based upon their differences in time of year, origin, and trajectory with respect to the snow boundary. The first case examined was a typical Alberta Clipper that developed in northwesterly flow in early March 2005, crossing from north to south of the snow line during its evolution. The second was a lee-cyclogenesis case that developed east of the Rockies and propagated to the northeast thereafter, crossing from south to north of the snow boundary. The immediate effect of snow removal (ie, occurring within one week following removal) in the two cases is shown in Fig. 1.

Regions of warm 1000 hPa temperature anomalies are observed in both cases and are broadly collocated with the area over which snow was removed. For the March 2005 case, the snow line ran northwest to southeast over the continental United States, a shape which is imitated in the 90th percentile removal simulation snow line located farther north (Fig. 1a). The 1000 hPa warm anomalies developed over the removal of snow and were strongest over the upper Midwest and

238 southern Canada. The anomalies extend farther south than the area of snow removal, presumably
239 a result of mixing and advection of these anomalies by the circulation.
240 The January 1996 case exhibited a snow boundary which cut more directly west-east across
241 the continent, and in this case the temperature anomalies were characterized by three local
242 maxima over Nevada, the Great Plains, and southern Ontario (Fig. 1b). In both cases weak
243 negative height anomalies accompanied the warm temperature anomalies at 1000 hPa, consistent
244 with the notion that a surface warm anomaly produces a cyclonic QGPV/height anomaly.
245 *3.1 March 2005 Case*
246 The cyclone in this case began as a depression aligned along a region of strong
247 baroclinicity on 6 March which subsequently slid southeastward and amplified one day later over
248 Wisconsin (Fig. 2a-b). By that time the region of strongest baroclinicity was located just north of
249 the snow line, and the cyclone tracked roughly along the snow line as it propagated and
250 amplified. The cyclone weakened slightly on the 8th (Fig. 2c), subsequently deepening rapidly
251 (likely aided by ingestion of warm, moist air from over the Atlantic Ocean) as it propagated to
252 the northeast on 9 March (Fig. 2d). By this time the cyclone also exhibited a well-developed
253 thermal structure including a prominent cold front.
254 In the 90th percentile simulation, negative $z''$ anomalies developed near the surface just to
255 the east of where the cyclone began to develop on the 6th, over the region of snow removal and
256 farther to the south as well (Fig. 3a). The negative height anomalies strengthened thereafter,
257 overlapping with the cyclone center (and therefore deepening the height minimum of the
258 cyclone) on the 7th and 8th (Fig. 3b-c). Regions of positive height anomalies developed on 8
259 March, near the modified snow boundary, strengthening on the 9th in the cyclone's northwest
260 quadrant (Fig. 3d). Supporting our initial hypothesis, positive temperature anomalies were

roughly collocated with the negative height anomalies on 6-7 March (Fig. 4). Later in the cyclone lifecycle, however, the direct relationship between the temperature and height anomalies weakens. By 8 March, and increasingly by 9 March, the correspondence between the temperature and height anomalies is rather poor, with the warm anomalies remaining in the area of snow removal, while positive height anomalies developed over much of eastern Canada over the snow-covered region and negative height anomalies formed south of the snow boundary in the Midwest United States (cf. Fig. 3d, Fig. 4d).

Cross sections of height and temperature anomalies ($z''$ and $T''$), taken at the times and locations marked in Fig. 4b,d, indicate that on 7 March the 1000 hPa negative height anomaly observed over the cyclone center extends only to 800 hPa, at which point the sign of the height anomalies reversed to positive north of 45°N. (Fig. 5a). The surface warm anomaly is similarly shallow, with a very weak temperature response in the mid and upper troposphere (Fig. 5c). Two days later on 9 March, the negative height anomaly at the surface has weakened substantially, while a stronger positive height anomaly has developed through much of the troposphere, at some points extending all the way to the surface, such as at 50°N (Fig. 5b). The surface warm anomaly observed on 7 March has weakened in magnitude as well, and now extends to about 500 hPa, tilting slightly northward with increasing altitude (Fig. 5d). A negative temperature anomaly located from 200 – 300 hPa developed by this time, located just above the maximum in the positive height anomaly.

It therefore appears that early in the cyclone lifecycle, the removal of snow enhanced the cyclonic circulation near the surface. Later, this effect weakened as it was negated by a broad increase in heights above the surface. Upper-tropospheric cooling is observed from 200-300 hPa (consistent with presence of the height anomalies that are decreasing with height, Eqn 3)

revealing that, although weak, changing the lower boundary had an impact all the way to the tropopause. The structure of the height response to snow removal on 7 March resembles the Saharan heat low, a warm-core low pressure center that is strongest near the surface and transitions to an upper-level anticyclone near 700 hPa (Lavaysse et al. 2009). Heat lows are surface-driven, which may explain why their structure resembles the height response to snow removal. The anticyclonic anomaly subsequently strengthened over time as observed on 9 March, at some locations extending to the surface.

Cross sections of the height fields attained from inverting the combined temperature term ($z_T'' = z_\theta''+z_{st}''$) and relative vorticity components of the QGPV indicate that, as suspected, the temperature term is responsible for the majority of the strong, shallow height anomaly observed on 7 March (Fig. 6a-b). Above 800 hPa, the temperature and vorticity components both contribute to positive height anomalies north of 45°N, while the vorticity component produced negative anomalies to the south (Fig. 6c). Overall, the patterns of the height responses from $z_T''$ and $z_\zeta''$ are notably different, with the temperature contribution displaying strong variations with height, meaning it is overall baroclinic, while the relative vorticity contribution is more constant with height and thus overall barotropic. Further partitioning the temperature term into contributions from static stability and the surface temperature anomaly illustrates the strong cancellation between these two terms (Fig. 7). The warm 1000 hPa temperature anomaly is treated as a positive QGPV anomaly, inducing a cyclonic height anomaly as anticipated (Fig. 7a). The vertical structure of a positive temperature anomaly that decreases with height increases the environmental lapse rate, reducing the stability and therefore producing a negative QGPV anomaly. Correspondingly, inversion of $q_{st}''$ produces an anticyclonic height anomaly (Fig. 7b). The sum of these two opposing aspects related to temperature and stability indicates that, at this

time and location, the cyclonic effect of the surface temperature anomaly is just slightly stronger than the anticyclonic anomalies produced by the stability term, leading to a net negative anomaly at the surface (Fig. 7c). Above 700 hPa, the stability influence is stronger and positive height anomalies result (Fig. 7c and Fig. 6b, which both show $z_T''$ but at different contour intervals). Similar cancellation was observed by Holopainen and Kaurola (1991) using a prescribed surface temperature and vertical temperature distribution, although the cancellation occurred higher in the troposphere near 500 hPa.

Two days later on 9 March, the cyclonic 1000 hPa height anomaly over the cyclone center weakened, due to a weaker negative anomaly associated with the $z_T''$ term (Fig. 8a-b). Simultaneously, the $z_\zeta''$ term contributed more strongly to the height field, producing positive height anomalies throughout most of the troposphere, with maxima from 300-400 hPa from 35-45°N, and from 800-1000 hPa at 50°N (Fig. 8c). Overall the height response appears more dominated by the relative vorticity contribution to development, in contrast to the 7 March cross section in which the surface temperature effect was strongest.

The influence of the surface warm anomaly produced by removing snow therefore appears to incite a direct effect observed early in the cyclone lifecycle, an effect which deepens the developing cyclone. As the cyclone matures, however, the relative vorticity field produces an anticyclonic anomaly that extends to the surface and weakens the surface cyclone in its northwest quadrant (Fig. 3d). Thus while the direct response to the warm surface anomaly produced by removing snow acts according to our initial hypothesis, the response in the mid and upper troposphere induced by the vorticity response to snow removal also influences the development of the surface cyclone.

*3.2 January 1996 Case*

The January 1996 cyclone developed predominantly south of the snow line, in contrast to the March case which originated north of the snow line and propagated southeastward across it. The January case also developed in the wake of a predecessor cyclone, which was not the case for the March event. On 25 January, the cyclone was a small depression located in the central United States just south of the snow boundary and in a broad region of baroclinicity (Fig. 9a). The system propagated eastward over the next two days, its height minimum crossing to just north of the snow boundary on 27 January (Fig. 9b-c). At this time the cyclone also displayed a typical thermal structure including a warm sector, warm and cold fronts. One day later, the cyclone continued to deepen and also expanded notably in its horizontal extent, with its center located over the snow boundary in eastern Maine (Fig. 9d).

As in the previous case, negative 1000 hPa height anomalies result from the removal of snow, located over and south of the region where the snow was removed in the 90$^{th}$ percentile simulation (Fig. 10). On 25 January, positive height anomalies were located north of the modified snow boundary over eastern Canada, over the northern portion of the predecessor cyclone (Fig. 10a). From January 25-26 negative height anomalies developed to the east of the developing cyclone in the central US, with weakly negative anomalies located over the cyclone center (Fig. 10a-b). By 26 January, the positive anomalies observed over eastern Canada a day earlier had either weakened or propagated out of the model domain, along with the predecessor cyclone. On 27 January a strong couplet of negative and positive anomalies developed, straddling the amplifying cyclone located over Michigan, whose center was now located directly over the region of snow removal (Fig. 10c). By 28 January, the positive height anomalies west of the cyclone center on the 27$^{th}$ had expanded and appeared to have been advected southeastward by the cyclonic circulation of the system on its western edge (Fig. 10d). A region of negative

353 height anomalies is observed north of the cyclone center, having weakened substantially
354 compared to one day prior. The prevalence of negative height anomalies early in the cyclone
355 lifecycle, which transitions to a mix of positive and negative anomalies when the cyclone
356 matures, is a common element between the two cases, while the exact position of the anomalies
357 with respect to the cyclone center differs.

358 On 25 January, surface warm anomalies were roughly collocated with the negative height
359 anomalies where snow was removed, as in the March case (Fig. 11a). Thereafter, however, a
360 direct correspondence between the anomalous temperature and height fields is not apparent,
361 with, for instance, very strong warm anomalies located northwest of the cyclone on 26 January,
362 where only weakly negative or neutral height anomalies were observed (cf. Fig. 11b, Fig. 10b).
363 Warm anomalies remained within the region of snow removal over the Great Plains and upper
364 Midwest through 28 January, while the height anomalies underwent a substantially different
365 evolution as the cyclone amplified and propagated eastward. This behavior is suggestive of a
366 stronger influence of the stability and relative vorticity contributions to the height field in this
367 case, which obscured the correspondence between surface temperature anomalies and height
368 anomalies observed more clearly in the March 2005 case. We note that there is no *a priori* reason
369 to expect a direct correspondence between the height and surface temperature fields, but that the
370 presence of such a relationship was suspected to be characteristic of the impact of snow removal
371 on the circulation as suggested by Fig. 1.

372 Cross sections of height and temperature anomalies on 25 January show that the negative
373 height anomalies and warm anomalies were greatest near the surface and gradually weakened
374 with altitude, though not as rapidly as observed on 7 March in the previous case (cf. Fig. 12a,c,
375 Fig. 5a,c). The height anomalies changed sign to positive near 600 hPa, peaking in strength at

300 hPa. Three days later on 28 January, the height response over the cyclone center (located at 45°N) reversed, with positive anomalies observed south of 50°N in the lower troposphere (Fig. 12b). The temperature anomaly pattern had also evolved into a broad, weak cold anomaly located near 40-45°N at the surface, tilting northward with altitude to about 350 hPa (Fig. 12d). Only a small remnant of the previously strong surface warm anomaly remained, centered just north of 45°N. QGPV inversion will investigate which terms contributed to this dramatic reversal of the temperature and height fields.

Cross sections of the $z_T''$ and $z_\zeta''$ contributions to the $z''$ field indicate that the former accounted for most of the negative height anomaly in the lower-troposphere and positive height anomalies in the mid-upper troposphere, as observed in the March case (Fig. 13a,b). The relative vorticity contribution to the height field reinforced that induced by the temperature term, particularly at upper levels (Fig. 13c). The deeper vertical extent of the warm anomaly in this case compared to the March case (Fig. 12c) coincides with a deeper vertical extent of the negative height anomalies from the surface into the troposphere. Three days later on 28 January, the $z_T''$ response reversed from its pattern on the 25th, and is associated with positive height anomalies in the lower troposphere and negative height anomalies above 600 hPa (Fig. 14a-b). The vorticity contribution to the height field had also changed and, by this time, accounted for the majority of the negative height anomalies observed throughout the troposphere north of 45°N and positive height anomalies at lower latitudes (Fig. 14c). In the net, the two components of the height field enhance one another near 40°N to produce the positive anomalies observed at 1000 hPa. The increase in the magnitude of the vorticity-induced anomalies later in the cyclone lifecycle is similar to that observed in the March case, although there is little similarity in the structure of the vorticity-induced height response between cases.

399 The complete sign reversal of the $z_T''$ anomalies over the course of the lifecycle, observed
400 only in the January case, is another notable difference between the cases (Fig. 12a,b). This
401 change could occur if the surface temperature anomaly changed sign from warm to cold, or if the
402 stability term dominates over the direct temperature effect through changes in the vertical
403 structure of the temperature field. While cold anomalies were observed in much of the lower
404 troposphere, anomalies at 1000 hPa were weak but positive at 45°N (Fig. 12d). Decomposing the
405 $z_T''$ term on 28 January reveals that the 1000 hPa temperature anomaly induced a
406 negative/cyclonic $z_\theta''$ anomaly, which was negated by a stronger, positive height anomaly
407 produced by the stability term ($z_{st}''$) from 1000-700 hPa (Fig. 15). The negative anomalies
408 produced by the surface temperature component are most likely driven by the nonlocal effect of
409 the broad warm anomalies observed to the west of the location of the cross section at 1000 hPa
410 (Fig. 11d). However, the stability term captures the vertical structure of the cold anomalies
411 observed more directly over the cyclone center (Fig. 12d), producing height rises where the
412 temperature anomalies decreased with altitude (Fig. 15b). The stability contribution is essentially
413 highlighting how a strong surface warm anomaly, or mid-tropospheric cold anomaly, increases
414 the environmental lapse rate and reduces the stability of the lower troposphere, creating a
415 negative QGPV anomaly and a positive height anomaly. How the removal of snow led to a cold
416 anomaly over the cyclone during its mature phase is not immediately clear, and suggests that
417 snow removal can lead to a variety of indirect and potentially opposing effects, likely related to
418 differences in the advection of temperature and vorticity between simulations.

419 **4. Discussion and Conclusions**

420 We have investigated the short-term atmospheric response to a northward-shifted snow
421 boundary during boreal winter for two cases selected for their differences regarding position

relative to the snow line, time of year and origin. We found that the opposing effects of a surface warm anomaly, which simultaneously produces a cyclonic QGPV anomaly and a negative static stability anomaly, heavily influenced the height response near the surface. Our results are consistent with those of Elguindi et al. (2005), who found that increasing snow cover over the Great Plains weakened weather systems and enhanced lower-tropospheric stability. Here, we posed the opposite problem and found an opposite result, with stronger surface cyclone minima and reduced static stability.

In both cases investigated, the overall impact of snow removal early in the cyclone lifecycle involved production of negative height anomalies which deepened the surface feature, while at upper levels positive height anomalies developed above the surface warm anomalies. The structure of the temperature and height fields in the nascent stage of the cyclone lifecycle in both cases is similar to the structure of 'thermal lows' that often develop over arid regions in the subtropics (Ramage 1971; Rowson and Colucci 1992). Thermal lows develop from strong surface heating and have a non-frontal cyclonic circulation, most commonly confined to below 700 hPa, with the circulation weakening and often becoming anticyclonic higher in the troposphere (Petty 2008), as observed in these two cases.

As the relative vorticity contribution to heights strengthened later in the cyclone lifecycle, the height response in both cases involved development of positive height anomalies west of the surface cyclone center (cf. Fig.3, Fig. 10). The advection of height anomalies by the circulation likely assisted in generating stronger horizontal gradients, subsequently increasing the magnitude of the anomalies themselves. At upper levels, the height response near the cyclone center differed. Whereas the March 2005 case was characterized by positive height anomalies, the January 1996 case featured a dipole of negative anomalies north of the cyclone center and

positive anomalies to its south. It is likely that the upper-tropospheric differences between the two cases are related to the change in the temperature structure near the cyclone center. The cold temperature anomalies observed on 28 January, associated with reduced thickness, would be consistent with lower heights above the temperature anomaly, producing a cyclonic anomaly at upper levels. In the March case, the temperature anomaly consistently contributed a cyclonic anomaly, while the vorticity term contributed an anticyclonic anomaly. Despite these differences, in both cases the relative vorticity response to snow removal strengthened later in the cyclone lifecycle, ultimately dominating the height response.

Our results are roughly consistent with what Ellis and Leathers (1998) found as well, namely that the inclusion of snow cools the surface and removal warms the surface. Their study used a one-dimensional snow pack model to investigate the dynamics within cold air masses, which assumed temperature advection by the large-scale circulation was minimal. Our study, in contrast, highlights the lifecycle-dependent evolution of the temperature response engendered by removing snow. We find that the advection of the initial height response to snow removal by the cyclone itself generated vorticity, which subsequently produced its own height response. We therefore note that, when analyzing changes in the circulation that arise due to changing snow cover, advection must be considered along with in-situ interactions between the surface and overlying atmosphere.

Through this analysis the initial hypothesis was confirmed; namely, that a surface warm anomaly would be produced by removing snow, and would lead to development of a cyclonic QGPV anomaly and negative height anomaly. Somewhat unexpectedly, the analysis also revealed that this effect is most notable early in the cyclone lifecycle and can be negated or enhanced by the response in the vorticity field. The interplay between the temperature and wind

468 responses when the lower boundary changes is thus further elucidated, suggesting that the overall
469 response of developing cyclones to snow removal may be a small residual of two substantial but
470 opposing forcings. The surface warm anomaly, being a surrogate positive PV anomaly, serves to
471 induce negative height anomalies. As in the March 2005 case, the surface warming can
472 simultaneously lead to increased heights aloft via hypsometry. These local height increases
473 induce an anticyclonic vorticity anomaly aloft whose influence can extend back down to the
474 surface and manifest itself as opposing positive height anomalies. Alternatively, a cold anomaly
475 developed in the lower troposphere in the January 1996 case near the cyclone center, suggesting
476 that mixing and advection of air masses can oppose the surface warm anomaly initially produced
477 by removing snow.

478 In sum, the effects of removing snow on the cyclone lifecycle are observed and quantifiable,
479 but are generally transient and, even at their strongest, rather limited in magnitude and effect.
480 Large, permanent changes to cyclone intensity and trajectory due to changes in the snow
481 boundary do not seem likely when the snow removal leads cyclogenesis on daily timescales. We
482 emphasize that the long-term, nonlocal impacts of a receding snow line were not the target of
483 this analysis and could still have a large effect on the circulation, but the immediate, direct
484 effects of snow removal appear to be relatively minimal through the mitigating responses of
485 various components of the circulation. It is important to note that just two cases have been
486 analyzed in this study, with the goal of exploring the possible ways in which snow removal *could*
487 affect the cyclone lifecycle. However, statistical analysis of a larger number of cases from the
488 same model case studies reveals a relatively similar effect across all cases (Clare et al.,
489 submitted). Additionally, other features of storm evolution, including precipitation type,
490 mesoscale "snow-breeze" circulations, or cloud microphysics were not investigated, and could

be influenced by the snow cover change. Future work could apply the same methods employed here to a larger sample of the simulations to better understand the average response of midlatitude cyclones to a northward-shifted snow boundary. Finally, we note that the nature of the conducted experiments is highly idealized, and does not consider any future changes to the background state, such as enhanced moisture and baroclinicity, induced by climate shifts unrelated to snow removal. Simulations in the future could combine snow-removal-induced changes with modifications to the background state, such as increased warming and moisture, to determine how the snow removal response interacts with a realistically modified background.

## Data Availability

All model outputs are being submitted to the Environmental Data Initiative (EDI) repository. In the meantime, model data can be accessed at: http://co2.aos.wisc.edu/data/snowcover/.

## Acknowledgements

The authors acknowledge support for this project by the University of Wisconsin Office of the Vice Chancellor for Research and Graduate Education Fall Research Competition and the National Science Foundation Climate and Large-Scale Dynamics program award (NSF AGS-1640452). We also acknowledge technical support from the UW Advanced Computing Initiative (ACI) Center for High Throughput Computing (CHTC). We would also like to acknowledge Dr. Michael Notaro for assistance with model simulations.

## References

514 Bretherton, F. B., 1966: Critical layer instability in baroclinic flows. *Quart. J. Roy. Met. Soc.*,
515 **92,** 325-334.
516
517 Brown, R. D., 2000: Northern Hemisphere snow cover variability and change, 1915-97,
518 *Journal of Climate*, **13**, 2339-2354, doi:10.1175/1520-0442(200)013<2339:NHSCVA>2.0.CO;2.
519
520 Brutel-Vuilmet, C., M. Menegoz, and G. Krinner, 2013: An analysis of present and future
521 seasonal Northern Hemisphere land snow cover simulated by CMIP5 coupled climate models.
522 *The Cryosphere*, **7**, 67-80, doi:10.5194/tc-7-67-2013.
523
524 Clare, R.M., Desai, A.R., Martin, J.E., Notaro, M., Vavrus, S.J., 2020: Extratropical
525 Cyclone Response to Projected Reductions in Snow Extent over the Great Plains, *J. Climate*,
526 #JCLI-D-20-0103, submitted.
527
528 Elguindi, B. Hanson, and D. Leathers, 2005: The effects of snow cover on midlatitude
529 cyclones in the Great Plains. *Journal of Hydrometeorology*, **6**, 263-279, doi:10.1175/JHM415.1.
530
531 Ellis, A. W., and D. J. Leathers, 1998: A quantitative approach to evaluating the effects of
532 snow cover on cold air mass temperatures across the U.S. Great Plains. *Wea. Forecasting,*
533 **13,** 688–701.
534
535 Ellis, A. W. and D. J. Leathers, 1999: Analysis of cold airmass temperature modification
536 across the US Great Plains as a consequence of snow depth and albedo. *Journal of Applied*
537 *Meteorology and Climatology*, **38**, 696-711, doi:10.1175/1520-
538 0450(1999)038<0696:AOCATM>2.0.CO;2.
539
540 Gan, T. Y., R. G. Barry, M. Gizaw, A. Gobena, and R. Balaji, 2013: Changes in North
541 American snowpacks for 1979-2007 detected from the snow water equivalent data of SMMR
542 and SSM/I passive microwave and related climatic factors. *Journal of Geophysical Research:*
543 *Atmospheres*, **118**(14), 7682-7697, doi:10.1002/jgrd.50507.
544
545 Holopainen, E. and Kaurola, J. 1991: Decomposing the atmospheric flow using potential
546 vorticity framework. *Journal of the Atmospheric Sciences*, **48**, 2614–2625.
547
548 Klingaman, N.P., B. Hanson, and D.J. Leathers, 2008: A Teleconnection between Forced
549 Great Plains Snow Cover and European Winter Climate. *J. Climate,* **21**, 2466–
550 2483, https://doi.org/10.1175/2007JCLI1672.1
551
552 Lavaysse, C., Flamant, C., Janicot, S. et al., 2009: Seasonal evolution of the West African
553 heat low: a climatological perspective. *Clim. Dyn.,* **33: 313.** https://doi.org/10.1007/s00382-
554 009-0553-4
555
556 Lemke, P., J. Ren, R. B. Alley, I. Allison, J. Carrasco, G. Flato, Y. Fujii, G. Kaser, P. Mote,
557 R. H. Thomas, and T. Zhang, 2007: Observations: Changes in Snow, Ice, and Frozen Ground. In:
558 *Climate Change 2007: The Physical Science Basis. Contribution of Working Group I to the*
559 *Fourth Assessment Report of the Intergovernmental Panel on Climate Change* [Solomon, S., D.

Qin, M. Manning, Z. Chen, M. Marquis, K. B. Avery, M. Tignor, and H. L. Miller (eds.)]. Cambridge University Press, Cambridge, United Kingdom and New York, NY, USA.

Manabe, S. and R. T. Wetherald, 1980: On the distribution of climate change resulting from an increase in CO2 content of the atmosphere. *Journal of Atmospheric Sciences*, **37**, 99-118, doi:10.1175/1520-0469(1980)037<0099:OTDOCC>2.0.CO;2.

Petty, G. W., 2008: A First Course in Atmospheric Thermodynamics. 337 p. Sundog Publishing, Madison, WI.

Ramage, C.S., 1971: Monsoon Meteorology. Academic Press, New York, 296 p.

Ross, B. and J.E. Walsh, 1986: Synoptic-Scale Influences of Snow Cover and Sea Ice. *Mon. Wea. Rev.,* **114**, 1795–1810, https://doi.org/10.1175/1520-0493(1986)114<1795:SSIOSC>2.0.CO;2

Rowson, D. R. and S. J. Colucci, 1992: Synoptic climatology of thermal low-pressure systems over south-western north America. *International J. of Climatology*. **12**, 529-545.

Rydzik, M. and A. R. Desai, 2014: Relationship between snow extent and midlatitude disturbance centers. *Journal of Climate*, **27**, 2971-2982, doi:10.1175/JCLI-D-12-00841.1.

Skamarock, W. C., Klemp, J. B., Dudhia, J., Gill, D. O., Liu, Z., Berner, J., ... Huang, X. –yu, 2019: A Description of the Advanced Research WRF Model Version 4. No. NCAR/TN-556+STR doi:10.5065/1dfh-6p97

Sobolowski, S., G. Gong, and M. Ting, 2010: Modeled climate state and dynamic response to anomalous North American snow cover. *Journal of Climate*, **23**, 785-799, doi:10.1175/2009JCLI3219.1.

596 **Tables**
597

| Modeling Center (or Group) | Institute ID | Model Name | Horizonal Res. (°lon × °lat) | No. Vertical Levels |
|---|---|---|---|---|
| Commonwealth Scientific and Industrial Research Organization (CSIRO) and Bureau of Meteorology (BOM), Australia | CSIRO-BOM | ACCESS1.0 | 1.875 × 1.25 | 38 |
| National Center for Atmospheric Research | NCAR | CCSM4 | 1.25 × 1.0 | 26 |
| Centre National de Recherches Météorologique/Centre Européen de Recherche et Formation Avancée en Calcul Scientific | CNRM-CERFACS | CNRM-CM5 | 1.4 × 1.4 | 31 |
| Commonwealth Scientific and Industrial Research Organization in collaboration with Queensland Climate Change Centre of Excellence | CSIRO-QCCCE | CSIRO-Mk3.6.0 | 1.8 × 1.8 | 18 |
| NASA Goddard Institute for Space Studies | NASA GISS | GISS-E2-H, GISS-E2-R | 2.5 × 2.0 | 40 |
| Met Office Hadley Centre | MOHC | HadGEM2-CC, HadGEM2-ES | 1.8 × 1.25 | 60 |
| Institute for Numerical Mathematics | INM | INM-CM4 | 2.0 × 1.5 | 21 |
| Atmosphere and Ocean Research Institute (The University of Tokyo), National Institute for Environmental Studies, and Japan Agency for Marine-Earth Science and Technology | MIROC | MIROC5 | 1.4 × 1.4 | 40 |
| Max Planck Institute for Meteorology | MPI-M | MPI-ESM-LR | 1.9 × 1.9 | 47 |
| Meteorological Research Institute | MRI | MRI-CGCM3 | 1.1 × 1.1 | 48 |
| Norwegian Climate Centre | NCC | NorESM1-M, NorESM1-ME | 2.5 × 1.9 | 26 |

598
599
600 Table 1: CMIP5 models used to determine the range of likely changes in the position of the
601 snow/no snow boundary through the year 2100.
602
603
604
605
606
607
608
609
610

611 **Figures**
612

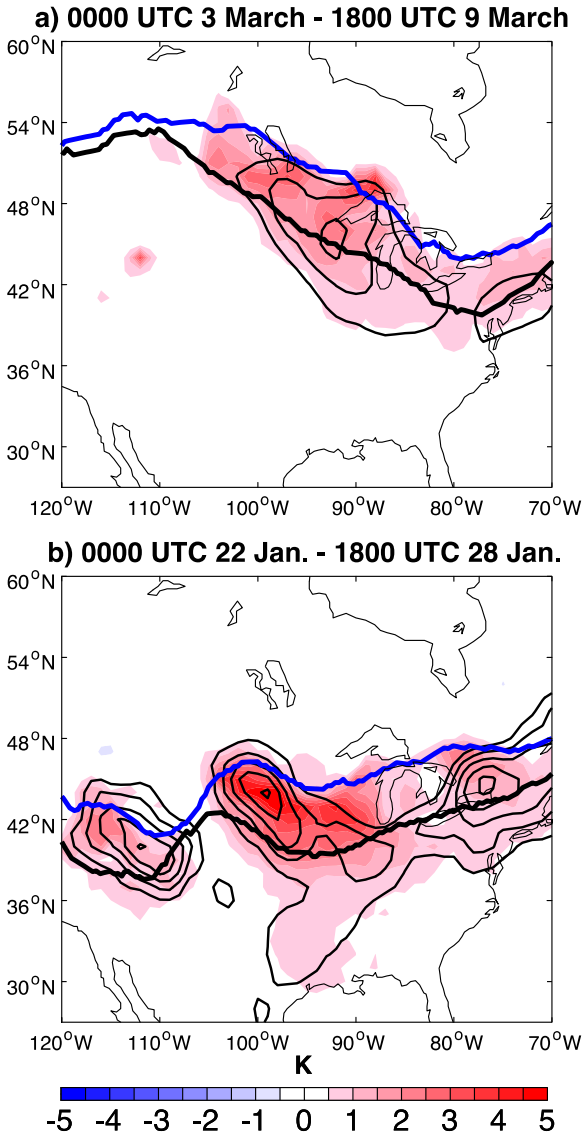


613
614
615 Figure 1: Location of snow boundary in control (bold black line), 90% removal simulations (bold
616 blue line) including simulated 7-day average 1000 hPa temperature anomaly in the color shading
617 and 7-day average 1000 hPa height anomalies, negative values only, beginning at -2 meters
618 contoured every 1 meter (thin black lines), for (a) 0000 UTC 3 March – 1800 UTC 9 March
619 2005 and (b) 0000 UTC 22 January – 1800 UTC 28 January 1996.

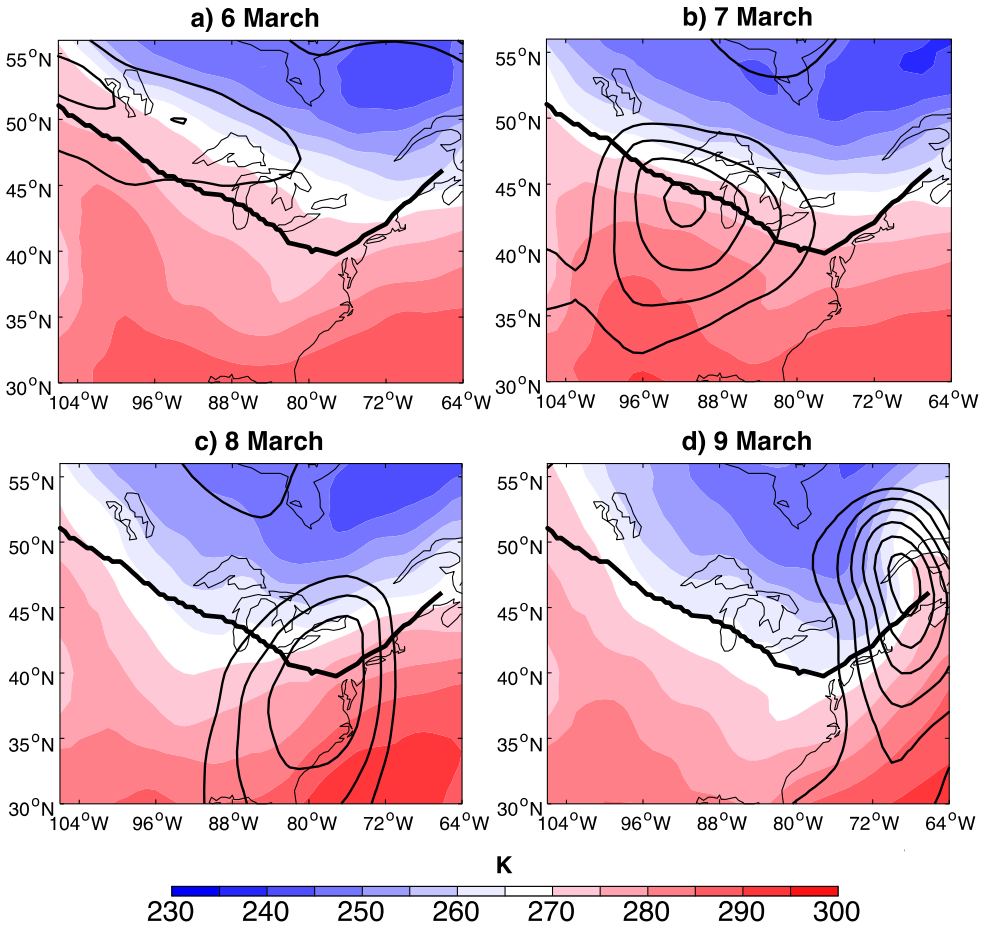


Figure 2: The color shading shows the daily mean 1000 hPa temperature, and the black thin contours show the 1000 hPa $z'$ field (anomalies calculated with respect to the 0000 UTC 3 March – 1800 UTC 9 March average), contoured every 25 meters starting at -25 meters, negative values only, for (a) 6 March through (d) 9 March, 2005. Fields are shown for the control simulation. The thick black line marks the location of the snow line in the control simulation.

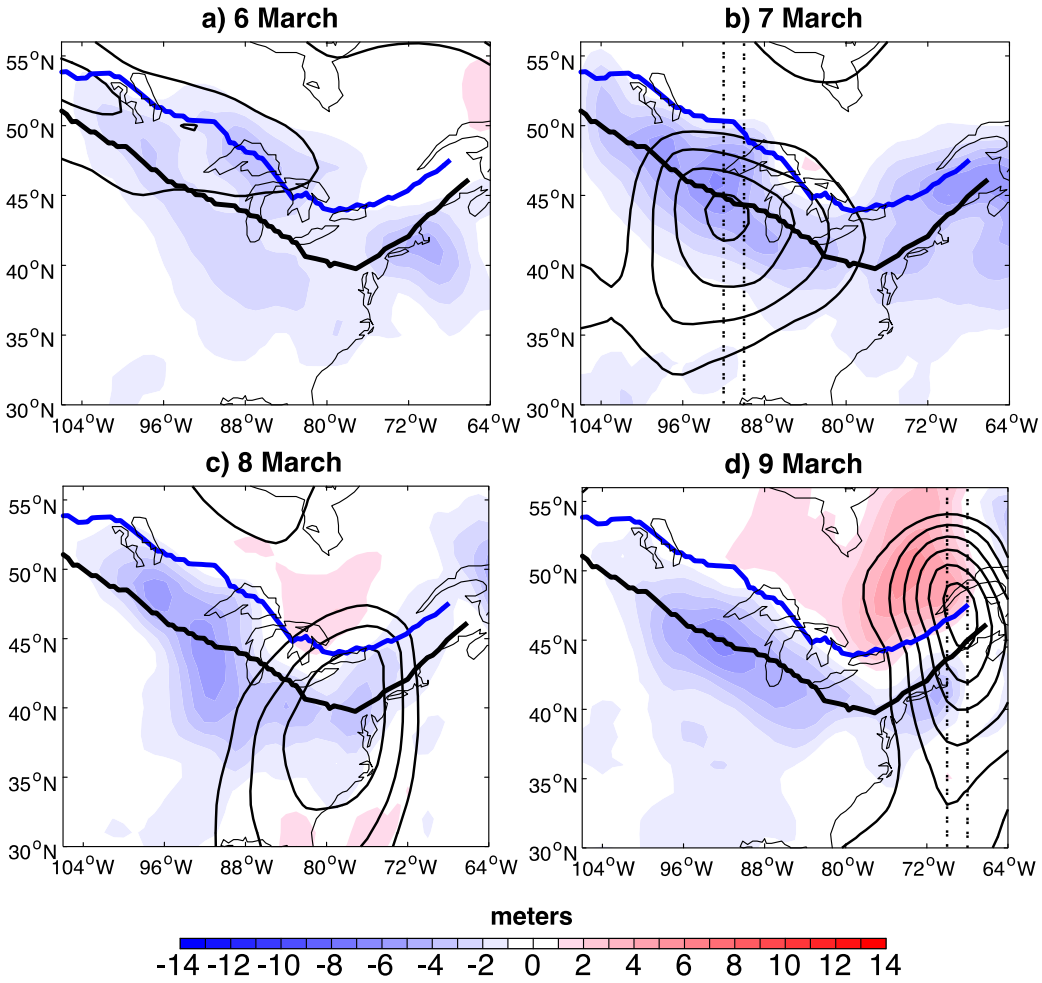


Figure 3: The color shading shows the daily mean 1000 hPa $z''$ field (anomalies calculated as the difference: 90th percentile simulation - Control simulation) at (a) 6 March – (d) 9 March, 2005. The thin black contours show the 1000 hPa $z'$ field, calculated with respect to the 0000 UTC 3 March – 1800 UTC 9 March average, contoured every 25 meters starting at -25 meters, negative values only. The thick black line marks the location of the snow line in the control simulation, while the thick blue line shows the snow line in the 90th percentile snow removal simulation. The dashed lines in panels (b) and (d) mark the location of cross sections presented in Fig. 5.

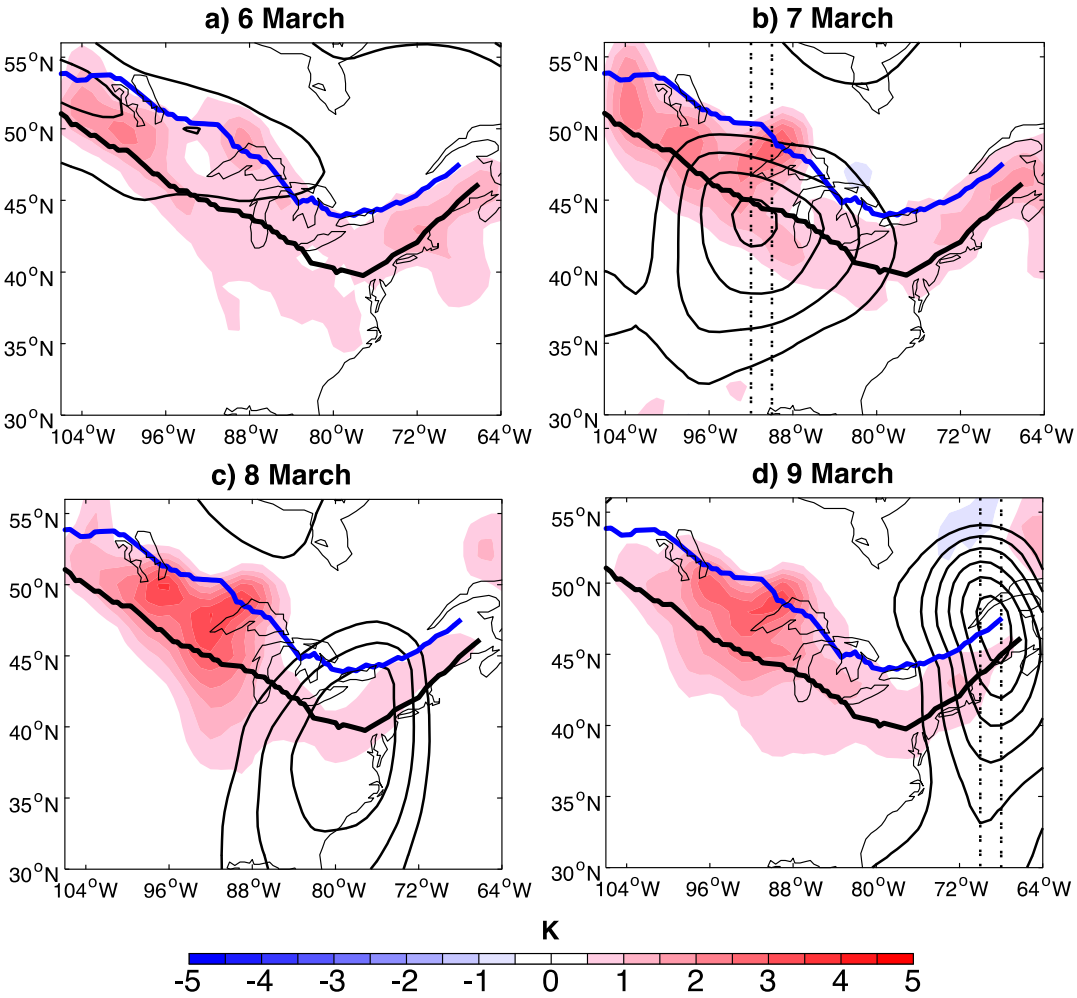


Figure 4: As in Figure 3 but with the color shading showing the daily mean difference in 1000 hPa $t''$ field.

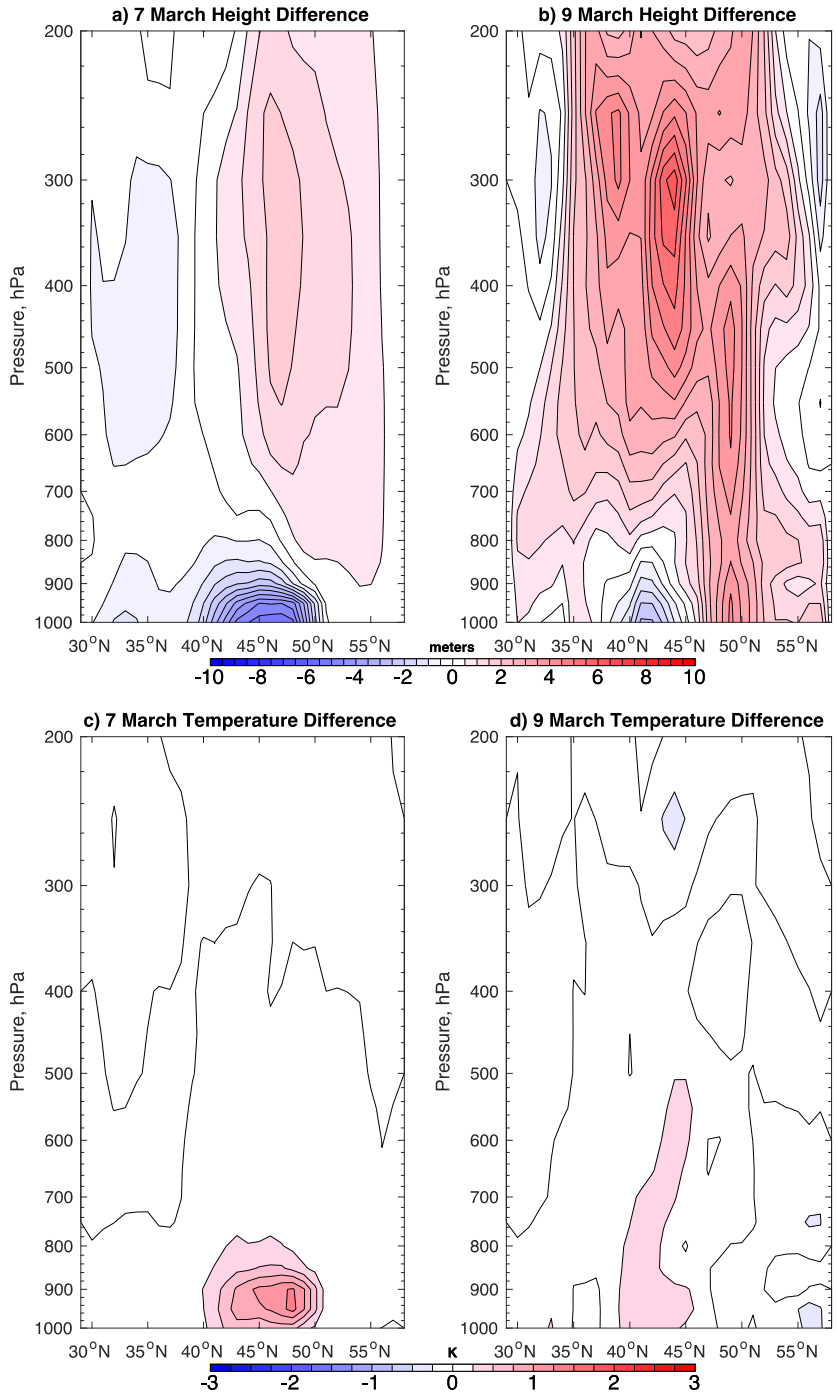


Figure 5: Cross sections of (a)-(b) $z''$ and (c)-(d) $t''$ taken at the locations and times shown in Fig. 4b,d. The left panels show cross sections taken on 7 March averaged from 268-270°E, and the right panels show cross sections taken on 9 March averaged from 290-292°E.

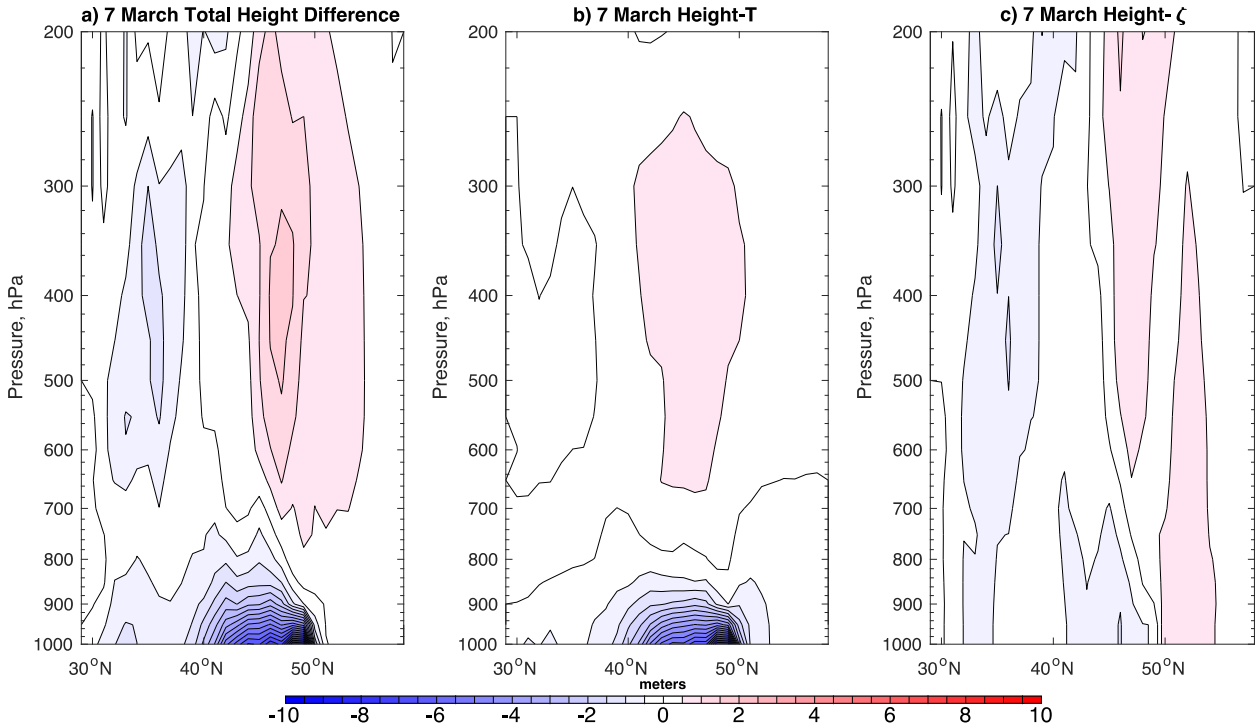


Figure 6: Cross-sections of the (a) total height change, (b) height change due to the $z_T''$ term, and (c) height change due to the $z_\zeta''$ term. All fields were averaged from 268-270°E (location shown in Fig. 4b) from 0000 – 1800 UTC 7 March 2005.

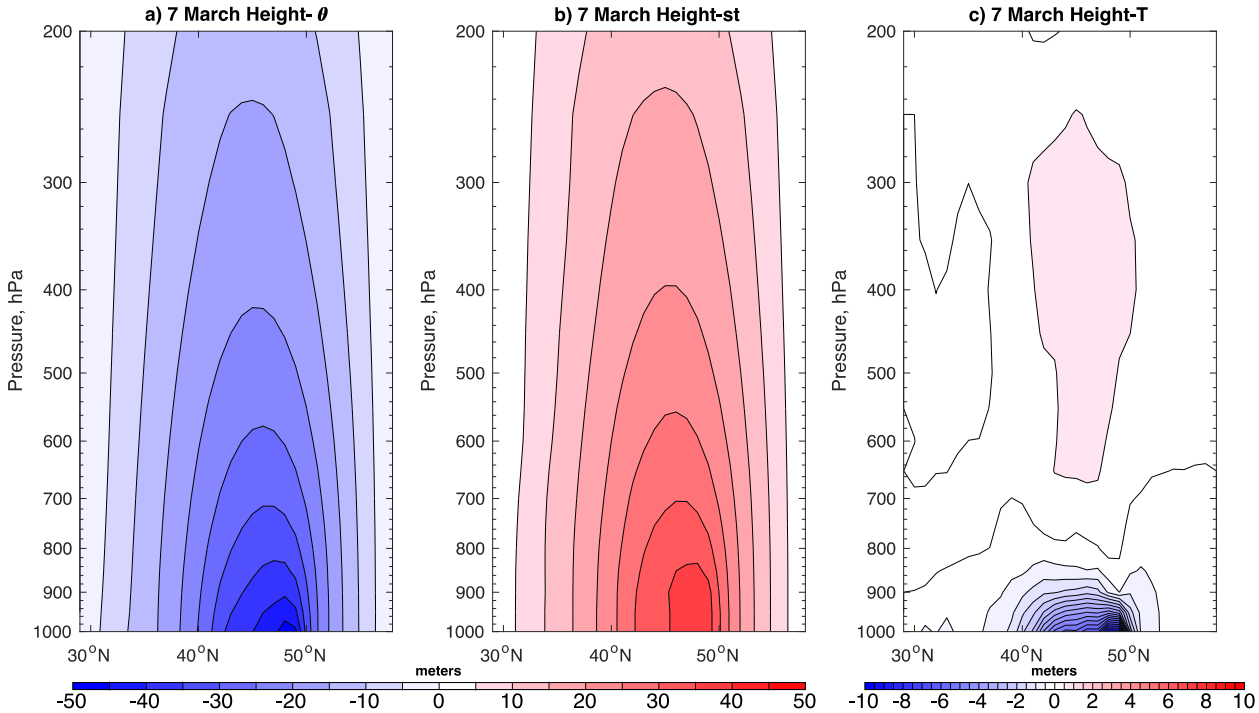


Figure 7: Decomposition of the $z_T''$ field into contributions from (a) $z_\theta''$ and (b) $z_{st}''$ on 7 March 2005. The net response, $z_T''$, is shown in panel (c). Note the change in the color scale compared to Figure 6, and that panel (c) is the same field as Fig. 6b.

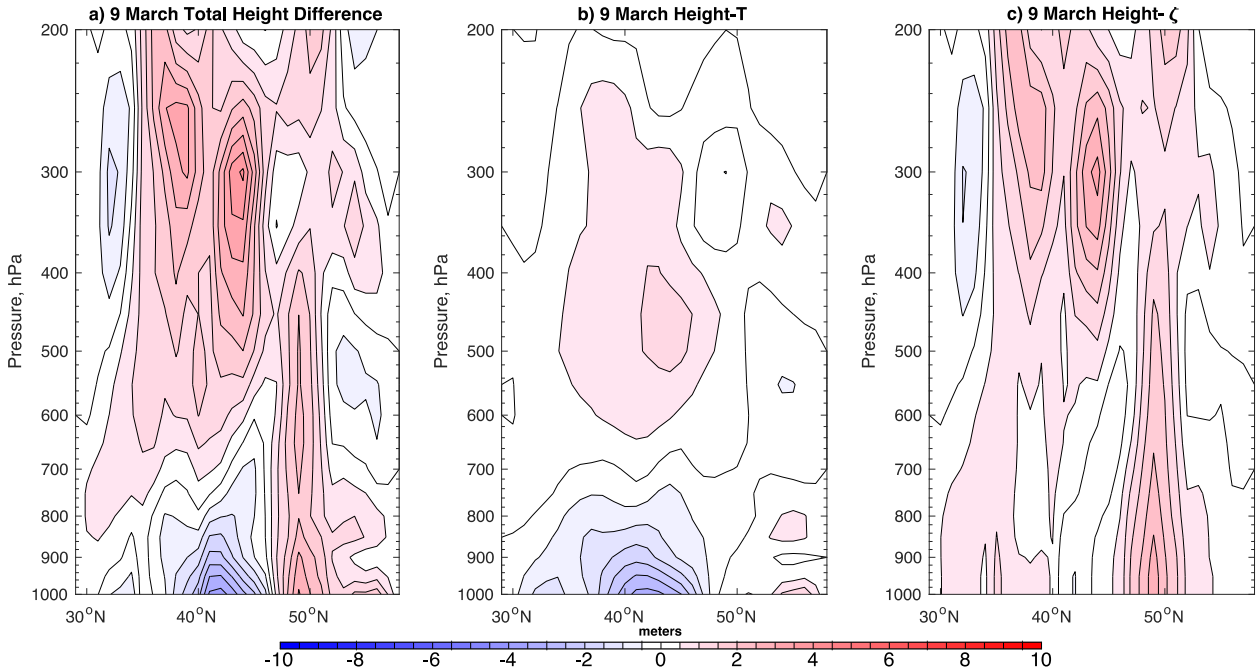


Figure 8: As in Fig. 6 but averaged from 0000 – 1800 UTC 9 March 2005, and over longitudes 290-292°E.

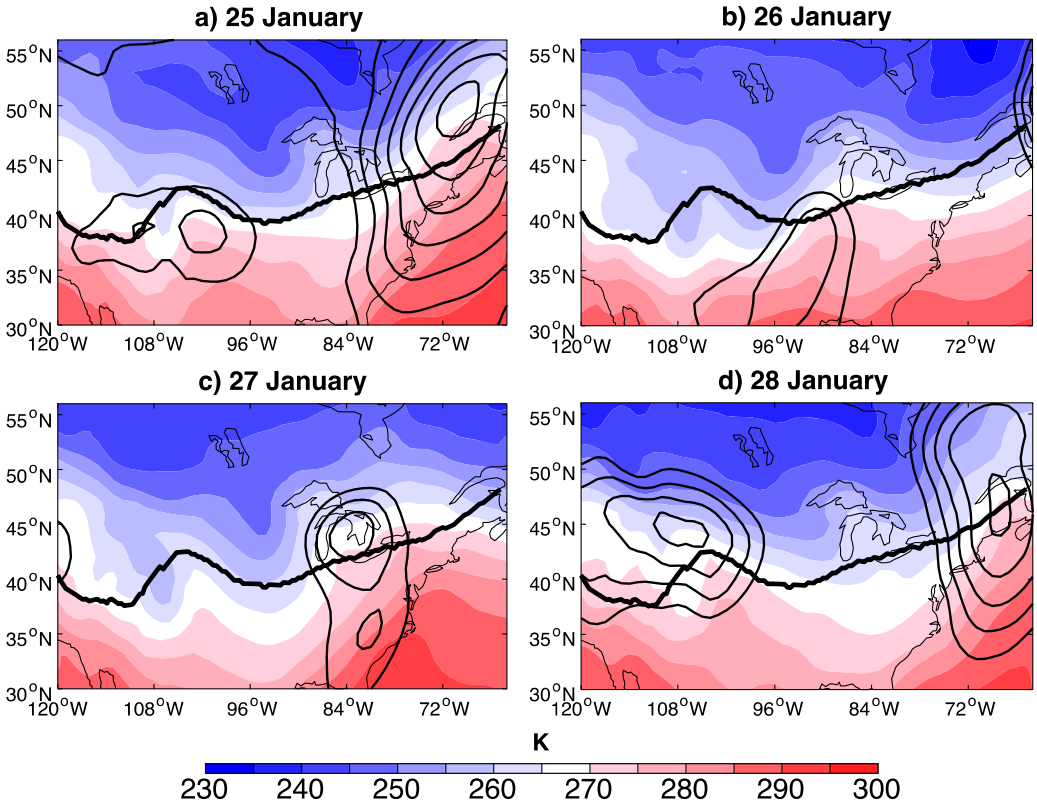


Figure 9: The color shading shows the daily mean 1000 hPa temperature, and the black thin contours show the 1000 hPa $z'$ field (anomalies calculated with respect to the 0000 UTC 22 January – 1800 UTC 28 January 1996 average), contoured every 25 meters starting at -25 meters, negative values only, for (a) 25 January through (d) 28 January, 1996. Fields are shown for the control simulation. The thick black line marks the location of the snow line in the control simulation.

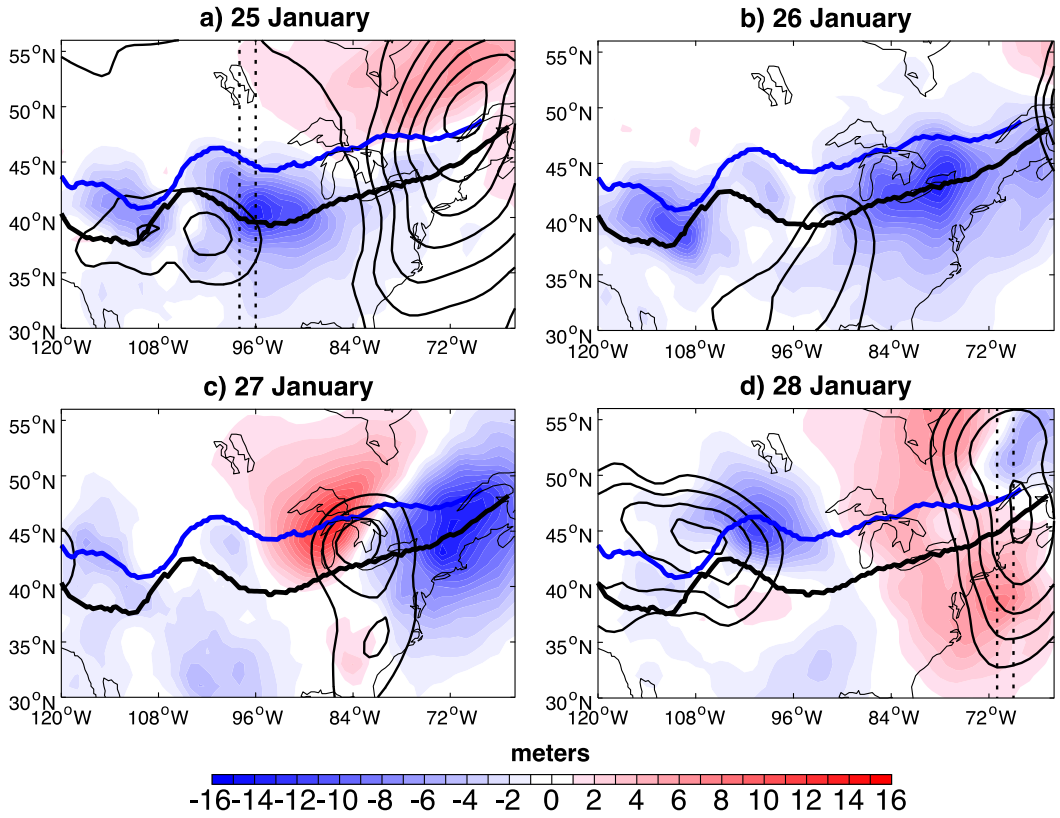


Figure 10: The color shading shows the daily mean 1000 hPa $z''$ field (anomalies calculated as the difference: 90th percentile simulation - Control simulation) at (a) 25 January – (d) 28 January, 1996. The thin black contours show the 1000 hPa $z'$ field, contoured every 25 meters starting at -25 meters, negative values only. The thick black line marks the location of the snow line in the control simulation, while the thick blue line shows the snow line in the 90th percentile snow removal simulation. The dashed lines in panels (a) and (d) mark the location of cross sections presented in Fig. 12.

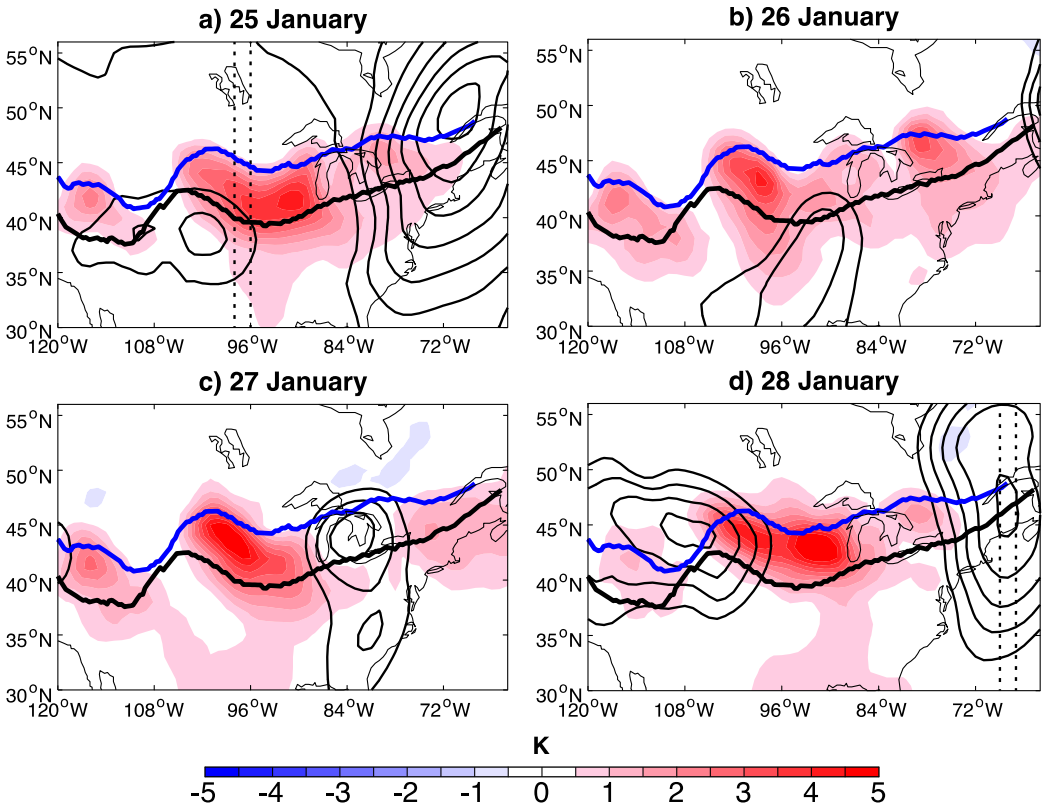


Figure 11: As in Figure 10 but with the color shading showing the 1000 hPa $t''$ anomalies.

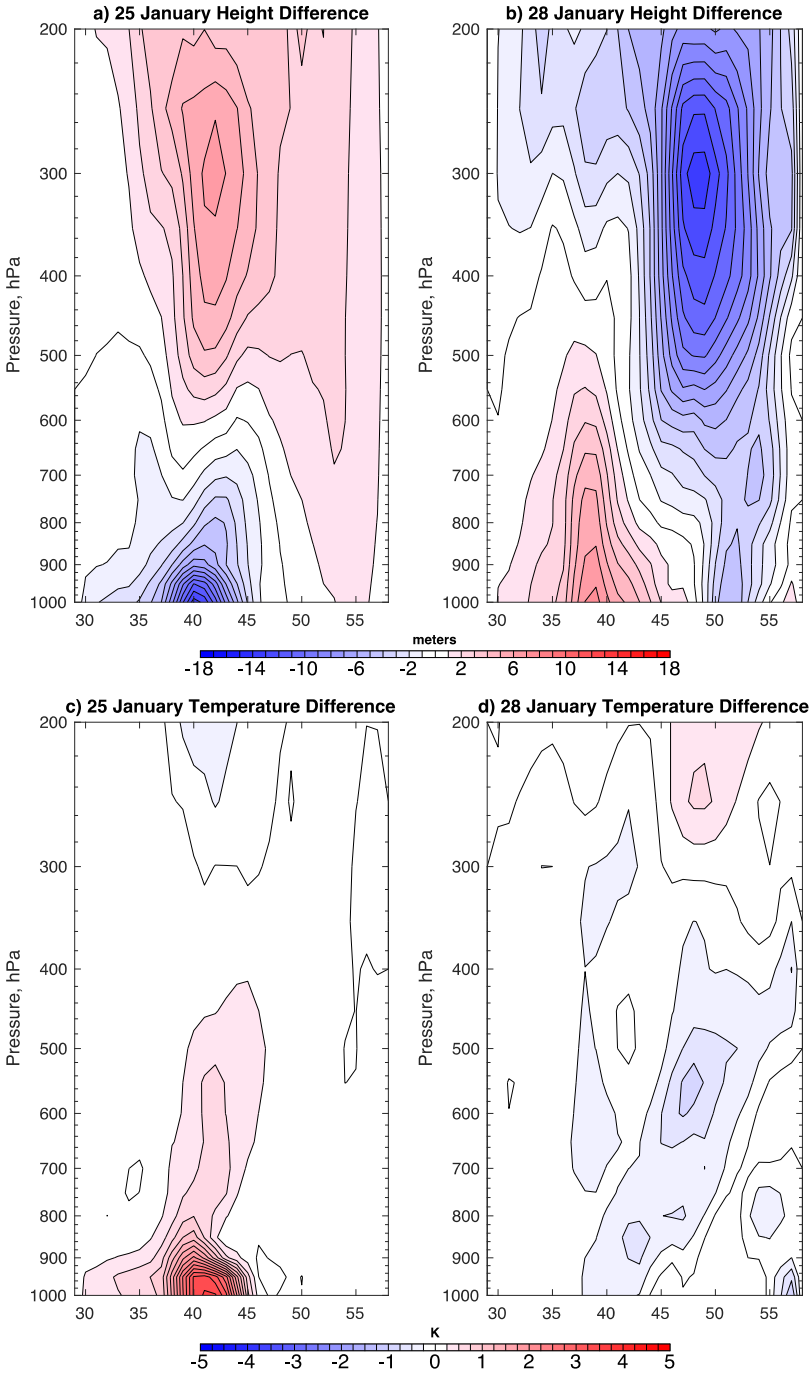


Figure 12: Cross sections of geopotential height (top) and temperature (bottom) averaged over the locations indicated in Fig. 11 on (a), (c) 25 January and (b), (d) 28 January, 1996.

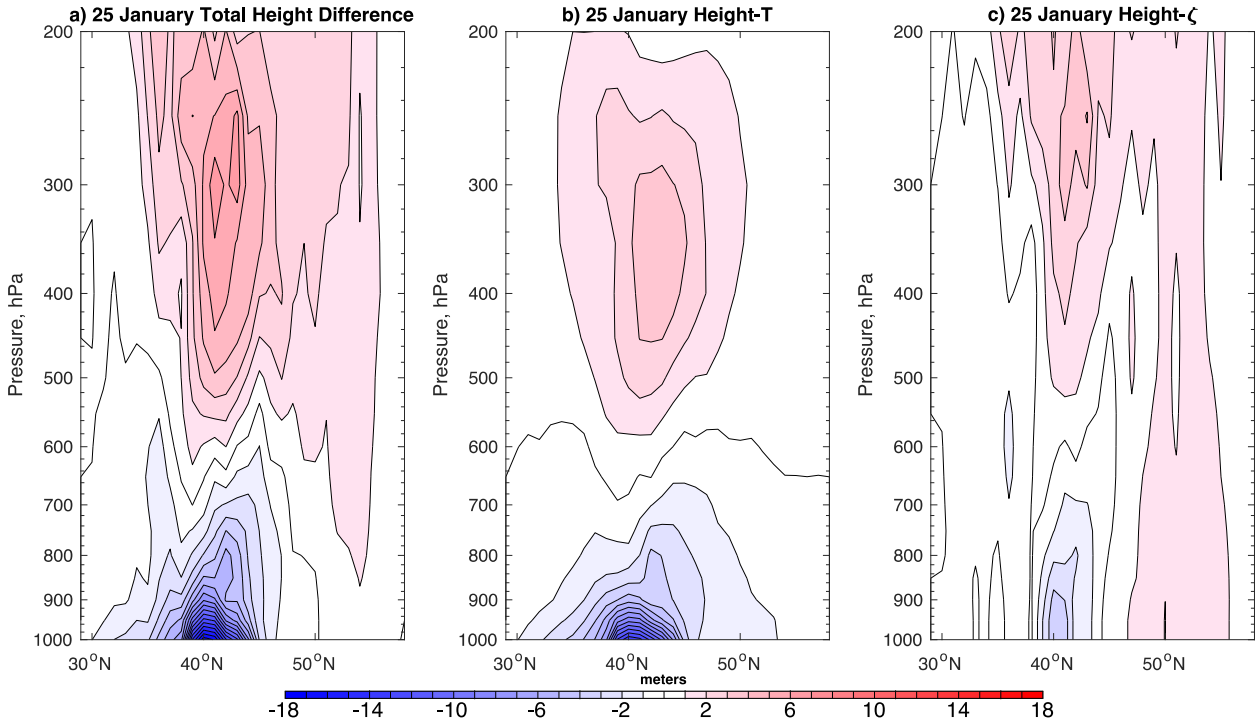


Figure 13: Cross-sections of the (a) total height change, (b) height change due to the $z_T''$ term, and (c) height change due to the $z_\zeta''$ term. All fields were averaged from 262-262°E (location shown in Fig. 11a) from 0000 – 1800 UTC 25 January 1996.

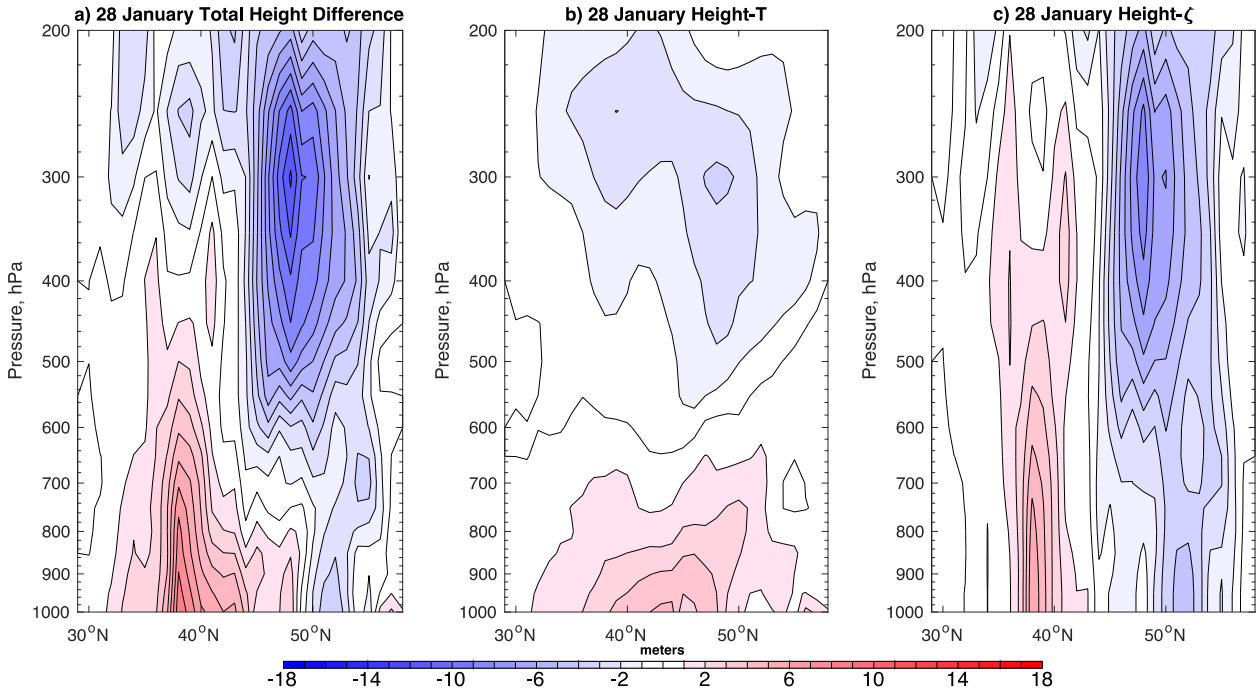


Figure 14: As in Fig. 13 but averaged from 289-291°E from 0000 UTC – 1800 UTC 28 January 1996.

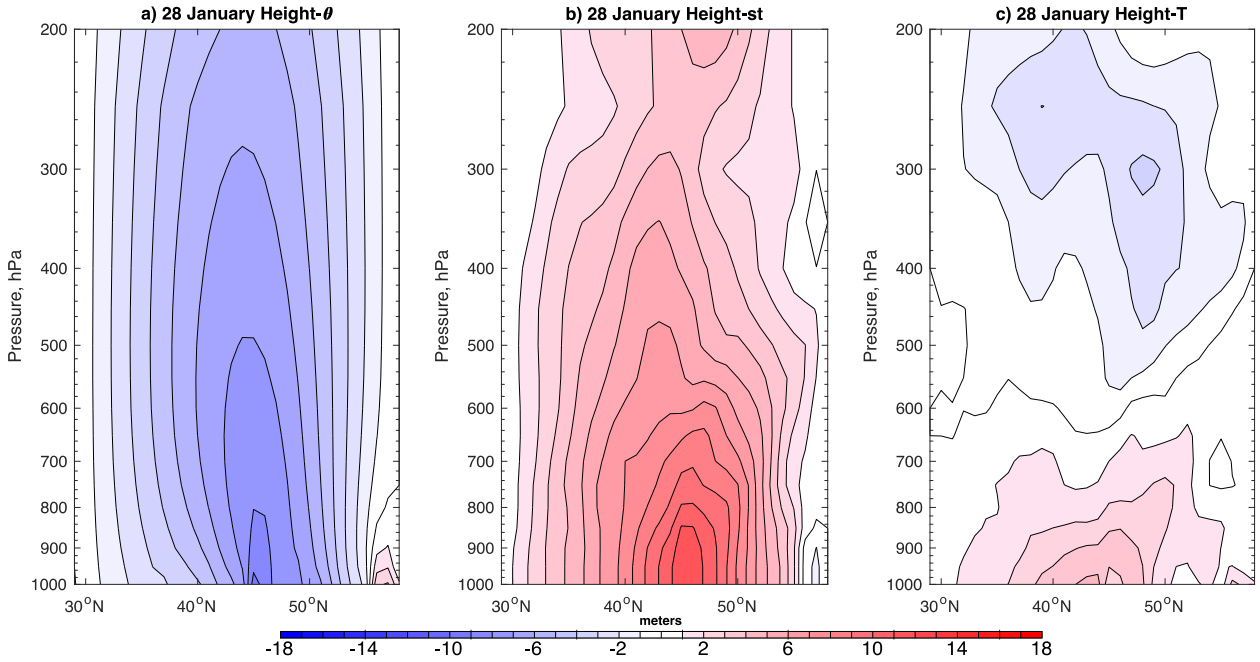


Figure 15: Decomposition of the $z_T''$ field into contributions from (a) $z_\theta''$ and (b) $z_{st}''$ on 28 January 1996. The net response, $z_T''$, is shown in panel (c).